Comparison of the sensitivity of air and dielectric modes in photonic crystal slab sensors

Snjezana Tomljenovic-Hanic,[1,2,*]Adel Rahmani,[3,1] M. J. Steel,[4,1] and C. Martijn de Sterke[1,2]

[1] *ARC Center of Excellence for Ultrahigh-bandwidth Devices for Optical Systems (CUDOS)*
[2] *School of Physics, University of Sydney, Camperdown, NSW 2006, Australia*
[3] *Department of Mathematical Sciences, University of Technology, Sydney, NSW 2007, Australia*
[4] *MQ Photonics Research Centre and Dept of Physics and Engineering, Macquarie University, NSW 2109, Australia*
*snjezana@physics.usyd.edu.au

Abstract: Optical cavities provide a route to sensing through the shift of the optical resonant peak. However, effective sensing with optical cavities requires the optimization of the modal quality factor, Q, and the field overlap with the sample, f. For a photonic crystal slab (PCS) this figure of merit, $M = fQ$, involves two competing effects. The air modes usually have large f but small Q, whereas the dielectric modes have high-Q and small f. We compare the sensitivity of air and dielectric modes for different PCS cavity designs and account for loss associated with absorption by the sensed sample or its host liquid. We find that optimizing Q at the expense of f is the most beneficial strategy, and modes deriving from the dielectric bands are thus preferred.

©2009 Optical Society of America

OCIS codes: (230.5298) Optical devices: Photonic crystals; (230.5750) Optical devices: Resonators

References and links

1. K. J. Vahala, "Optical microcavities," Nature **424**(6950), 839–846 (2003).
2. *Optical microcavities*, K. Vahala, ed. (World Scientific Publishing, 2004).
3. I. M. White, and X. Fan, "On the performance quantification of resonant refractive index sensors," Opt. Express **16**(2), 1020–1028 (2008).
4. I. M. White, J. Gohring, Y. Sun, G. Yang, S. Lacey, and X. Fan, "Versatile waveguide-coupled optofluidic devices based on liquid core optical ring resonators," Appl. Phys. Lett. **91**(241104), 1–3 (2007).
5. J. T. Robinson, L. Chen, and M. Lipson, "On-chip gas detection in silicon optical microcavities," Opt. Express **16**(6), 4296–4301 (2008).
6. F. Xu, V. Pruneri, V. Finazzi, and G. Brambilla, "An embedded optical nanowire loop resonator refractometric sensor," Opt. Express **16**(2), 1062–1067 (2008).
7. H.-C. Ren, F. Vollmer, S. Arnold, and A. Libchaber, "High-Q microsphere biosensor - analysis for adsorption of rodlike bacteria," Opt. Express **15**(25), 17410–17423 (2007).
8. J. Lutti, W. Langbein, and P. Borri, "High Q optical resonances of polystyrene microspheres in water controlled by optical tweezers," Appl. Phys. Lett. **91**(141116), 1–3 (2007).
9. M. Lončar, A. Scherer, and Y. Qiu, "Photonic crystal laser sources for chemical detection," Appl. Phys. Lett. **82**(26), 4648–4650 (2003).
10. E. Chow, A. Grot, L. W. Mirkarimi, M. Sigalas, and G. Girolami, "Ultracompact biochemical sensor built with two-dimensional photonic crystal microcavity," Opt. Lett. **29**(10), 1093–1095 (2004).
11. A. R. Alija, L. J. Martinez, P. A. Postigo, C. Seassal, and P. Viktorovitch, "Coupled-cavity two-dimensional photonic crystal waveguide ring laser," Appl. Phys. Lett. **89**(101102), 1–3 (2006).
12. N. A. Mortensen, S. Xiao, and J. Pedersen, "Liquid-infiltrated photonic crystals," Microfluid. Nanofluid. **4**(1-2), 117–127 (2008).
13. S.-H. Kwon, T. Sünner, M. Kamp, and A. Forchel, "Optimization of photonic crystal cavity for chemical sensing," Opt. Express **16**(16), 11709–11717 (2008).
14. D. F. Dofner, T. Hurlimann, T. Zabel, L. H. Frandsen, G. Abstreiter, and J. J. Finley, "Silicon photonic crystal nanostructures for refractive index sensing," Appl. Phys. Lett. **93**(181103), 1–3 (2008).
15. F. Bordas, M. J. Steel, C. Seassal, and A. Rahmani, "Confinement of band-edge modes in a photonic crystal slab," Opt. Express **15**(17), 10890–10902 (2007).
16. F. Bordas, C. Seassal, E. Dupuy, P. Regreny, M. Gendry, P. Viktorovitch, M. J. Steel, and A. Rahmani, "Room temperature low-threshold InAs/InP quantum dot single mode photonic crystal microlasers at 1.5 microm using cavity-confined slow light," Opt. Express **17**(7), 5439–5445 (2009).

17. S. Tomljenovic-Hanic, C. M. de Sterke, and M. J. Steel, "Design of high-Q cavities in photonic crystal slab heterostructures by air-holes infiltration," Opt. Express **14**(25), 12451–12456 (2006).
18. C. L. C. Smith, U. Bog, S. Tomljenovic-Hanic, M. W. Lee, D. K. C. Wu, L. O'Faolain, C. Monat, C. Grillet, T. F. Krauss, C. Karnutsch, R. C. McPhedran, and B. J. Eggleton, "Reconfigurable microfluidic photonic crystal slab cavities," Opt. Express **16**(20), 15887–15896 (2008).
19. U. Bog, C. L. C. Smith, M. W. Lee, S. Tomljenovic-Hanic, C. Grillet, C. Monat, L. O'Faolain, C. Karnutsch, T. F. Krauss, R. C. McPhedran, and B. J. Eggleton, "High-Q microfluidic cavities in silicon-based two-dimensional photonic crystal structures," Opt. Lett. **33**(19), 2206–2208 (2008).
20. B.-S. Song, T. Asano, and S. Noda, "Physical origin of the small modal volume of ultra-high-Q photonic double-heterostructure cavities," N. J. Phys. **8**(209), 1–12 (2006).
21. F. Intonti, S. Vignolini, V. Türck, M. Colocci, P. Bettoti, L. Pavesi, S. L. Schweizer, R. Wehrspohn, and D. Wiersma, "Rewritable photonic circuits," Appl. Phys. Lett. **89**(211117), 1–3 (2006).
22. S. Tomljenovic-Hanic, A. D. Greentree, C. M. de Sterke, and S. Prawer, "Flexible design of ultrahigh-Q microcavities in diamond-based photonic crystal slabs," Opt. Express **17**(8), 6465–6475 (2009).
23. T. Xu, M. S. Wheeler, H. E. Ruda, M. Mojahedi, and J. S. Aitchison, "The influence of material absorption on the quality factor of photonic crystal cavities," Opt. Express **17**(10), 8343–8348 (2009).

1. Introduction

Optical cavities have been developed in a wide range of geometries, exploiting a variety of resonant properties [1–3]. However, irrespective of the design, the ability of an optical cavity to confine light can be described by its quality factor, *Q*, and modal volume, *V*. *Q* is a measure of the temporal confinement of electromagnetic energy, or equivalently of the inverse of the loss rate of the cavity. On the other hand, *V* is a measure of the spatial confinement of electromagnetic energy, and to enhance the efficiency of light-matter interactions, in general one aims to minimize *V* while keeping *Q* as large as possible. Applications of optical cavities are as diverse as their properties, ranging from telecommunication to quantum electrodynamics. Our interest here is the area of bio-chemical sensing, which has attracted much attention recently [3–14]. These studies include a wide range of cavities such as a ring resonator [4,5], fiber coil resonator [6], microsphere [7,8] and photonic crystal slab [9–14].

Regardless of the platform, optical cavity-based sensors rely on the wavelength shift of the cavity resonance due to a change in the refractive index of an adjacent liquid. Upon addition of the sample to the liquid, the refractive index of the liquid changes slightly, shifting the cavity's resonant frequency. In biochemical applications, this change is formidably small. The shift is proportional to the energy fraction *f* of the resonant mode field that interacts with the sample [3,12], and thus it seems natural to try to maximize the fraction *f*. In addition to a large *f,* to obtain acceptable precision, cavity-based sensors must exhibit a frequency shift larger than the resonance linewidth. Since the linewidth is determined by the quality factor *Q*, the latter also plays a critical role and the relevant figure of merit to be maximized is actually the product $M = fQ$ [3,12]. We see this as follows. We define the sensitivity of the mode as the ratio of the frequency shift $\Delta\omega$ and the spectral linewidth $\delta\omega = \omega / Q$:

$$S = \frac{\Delta\omega}{\delta\omega}. \tag{1}$$

Here ω is the resonant frequency of the mode for the bare fluid which has index n_f. The introduction of the sample introduces a change in the fluid index Δn. To first order in Δn, (an extremely good approximation for these systems), the frequency shift is $\Delta\omega / \omega = f\left(\Delta n / n_f\right)$, where *f* is the energy fraction of the electric field in the fluid [12], so the sensitivity becomes:

$$S = fQ\frac{\Delta n}{n_f} = M \frac{\Delta n}{n_f}. \tag{2}$$

As mentioned above there is a wide range of optical cavities but the platform that enables the most compact optical cavities (and therefore the smallest sample volumes,) is the photonic crystal slab (PCS) [1]. In these structures, the light is confined in the plane of the slab by Bragg reflection and in the vertical direction by total internal reflection. Defect sites in the crystal slab can support localized states with frequencies falling inside the in-plane bandgap.

Provided the crystal is large enough, the primary loss mechanism for these states is out-of-plane leakage of near-vertical plane wave components. The modal volumes of PCS cavities are of order of a cubic wavelength. The high quality factor, small modal volume and precise design control available in PCS cavities promise applications in areas where strong light-matter interaction is essential for the device operation.

For PCS structures, the nature of the resonant mode depends on its location in the bandgap and this impacts the figure of merit M through two competing effects as follows. In a perfect crystal, the photonic eigenstates of the system are delocalized Bloch states and we can treat the localized modes of the cavity as superpositions of the Bloch states. The Bloch states of the uniform crystal near the lower band gap edge form *dielectric bands*, with the optical field mainly concentrated in the high index material. Cavity modes with resonant frequencies *close* to the lower band gap edge inherit this character, and have a small overlap between the field and the sample (holes), but typically have high-Q. In contrast, resonant modes close to the upper band gap edge have a large overlap between the field and the sample, but are usually low-Q modes as the field is mainly concentrated in the lower refractive index material reducing the effectiveness of the vertical confinement by total internal reflection [12]. Therefore, the figure of merit involves competing effects. Moreover, the favored mode may possibly depend on the class of cavity being considered.

In this paper, we compare the performance of the dielectric and air mode for two types of cavity. Though other related types of cavities exist [13], our results are obtained for structures that are examples of a larger class of cavities, a defect type [9,10,14–16] and double-heterostructure cavity (DH) [13,17–20]. For each exemplar cavity [15,17], we investigate the performance of dielectric and air bands and we determine which effect dominates.

2. Model and method

We consider a two-dimensional silicon PCS composed of a hexagonal array of cylindrical air holes with radius R, period a and thickness h. We investigate the performance of dielectric and air bands for two types of cavity: a confined band-edge point cavity [15] and a DH cavity [17]. Both cavities have been demonstrated experimentally [16,18,19]. Below we briefly describe those two designs. More details on the designs and numerical parameters for the calculations can be found in Refs [15,17].
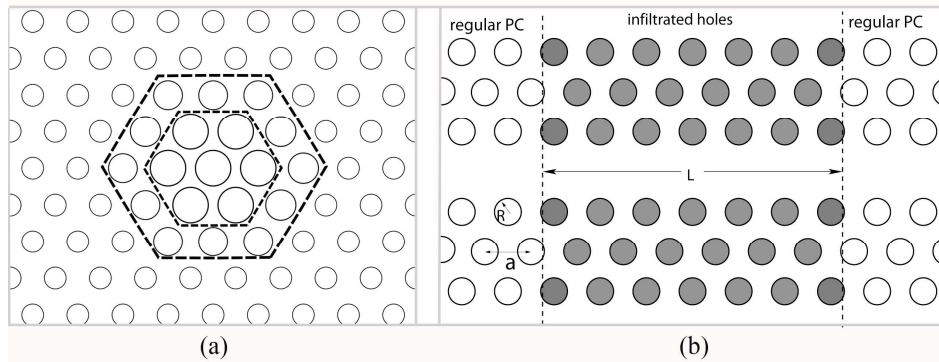

Fig. 1. (a) Schematic of a band edge cavity with a seven hole core and one adaptation ring. The hole radius decreases (increases) across the adaptation rings to confine a dielectric (air) band-edge mode (see text and [15] for details); (b) schematic of an infiltrated double-heterostructure cavity with $L = 6a + 2R$.

Confined band-edge point cavity: The structure consists of air holes ($R = 0.4a$) patterned in a slab of thickness $h = 0.42a$. The cavity is designed to trap dielectric or air band-edge Bloch states in a small region of the crystal by modifying the hole radius in the central *core* region of the crystal as described in [15]. Thus we can combine the high LDOS of the Bloch states with the small volume of the confined cavity. To confine a dielectric (air) mode the air hole radius in the core region R_c needs to be larger (smaller) than in the rest of the PCS. Here,

we use $R_c = 0.50a$ for the dielectric mode and $R_c = 0.36a$ for the air mode. Following the design of [15], adaptation rings are added around the core to smooth the variation in hole radius from the core to the bulk crystal and so increase the Q factor, with minimal change in the modal volume.

Double-heterostructure (DH): The structure has hole radius $R = 0.31a$ (air-mode) or $R = 0.29a$ (dielectric mode), with slab thickness $h = 0.6a$. There is a line defect in the form of a W1 waveguide in the Γ-K direction. Starting from a homogeneous PCS waveguide, the DH is formed by air-hole infiltration (indicated by the dark circles in Fig. 1(b)). The aim of this selective infiltration is to increase the average refractive index of the PCS which, to lowest order, has the effect of lowering the optical frequency of features in the photonic band structure of the infiltrated region with respect to that surrounding non-infiltrated region. The infiltrated region length is $L = 6a + 2R$, similar to previously demonstrated infiltration cavities [18,19]. The processing of air-hole infiltration can be done at any time after fabrication. It is even possible to address and infiltrate each hole separately [21], allowing further freedom and cavity design but we do not discuss here.

Beyond the obvious geometric differences, there is one fundamental distinction between the two architectures: in the confined band-edge cavity, the cavity region is defined by the silicon structure with its smoothly graded rings of holes, and all holes are infiltrated with the fluid which occupies a large region including and surrounding the cavity. In the DH case, the cavity is *defined* by the fluid itself, which only infiltrates selected holes along a region of length L, see Fig. 1(b). The two structures are thus suited to somewhat different scenarios: the band-edge cavity would allow continuous sensing of a flowing fluid, where the fluid volume was small but not critically so. In contrast, the DH cavity which requires precise fluid placement, would be useful for very small fluid volumes but would be difficult to operate in a dynamic fashion with a continuously flowing fluid.

The cavity properties, including quality factors and resonant frequencies, are evaluated using the three-dimensional finite-difference time-domain (FDTD) method. The computational parameters are similar to those used in Refs [15]. and [17], but of course as compared with these earlier studies, at least some of the holes are now fluid-filled. For the band-edge cavity this results in smaller Q due to the smaller refractive index contrast between the slab and the holes. On the other hand infiltrating the holes enables high-Q heterostructures because it allows for the *mode-gap* operation that relies on the refractive index perturbation [17]. The modal volumes of the resonant modes are calculated using the standard definition based on the electric energy density $U(\mathbf{r}) = \varepsilon(\mathbf{r})|\mathbf{E}(\mathbf{r})|^2 /2$ as:

$$V = \iiint d^3\mathbf{r} \; \frac{U(\mathbf{r})}{\max\left[U(\mathbf{r})\right]}. \tag{3}$$

3. Results

We calculate the resonant frequencies and total quality factors first without the presence of the sample. We then calculate the resonant frequencies and quality factors in the presence of the sample and find the sensitivity from Eq. (1). In Fig. 2, we show the sensitivity versus the refractive index change caused by the presence of the sample. Although there is no "standard" detection limit here we chose $S = 0.5$, at which the frequency shift is half the resonance linewidth. The solid horizontal line in Fig. 2 denotes this detection limit. It is nominally possible to detect any Δn for which S is above this line. In accord with Eq. (2), the sensitivity is proportional to Δn, with the detection limit determined by the merit factor M. From Fig. 2(a), we see that the detection limit of the band edge mode cavity is $\Delta n = 4 \times 10^{-6}$ for the dielectric mode and 2×10^{-5} for the air-mode. In Fig. 2(b) the detection limit for the DH cavity is 1.6×10^{-5} for the dielectric and 3.0×10^{-5} for the air-mode. For both cavities the sensitivity is larger for the dielectric mode than for the air mode. This is because the Q of the dielectric mode is much larger than that of the air-mode.
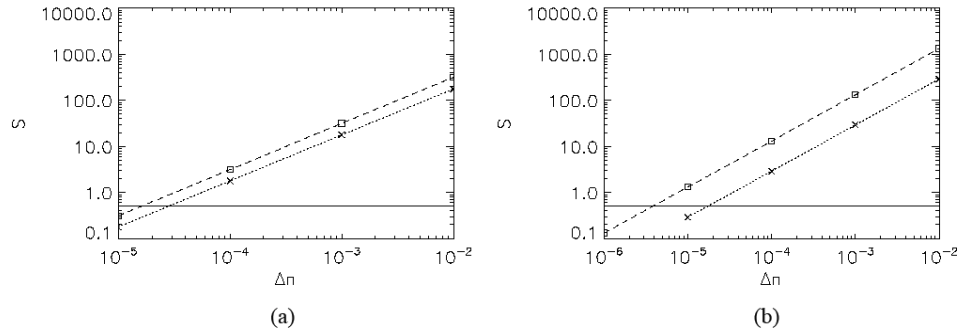
Fig. 2. Sensitivity of the air-mode (crosses) and dielectric mode (squares) for the (a) double-heterostructure type cavity and (b) band edge cavity as a function of the refractive index change. The solid horizontal line represents the detection limit.

The results for Q, f and M are summarized in Table 1. With the band edge cavity mode, for the air mode $Q = 8.8 \times 10^4$ and $f = 44\%$, while for the dielectric mode $Q = 1.3 \times 10^6$ and $f = 14\%$. Thus the larger overlap with the sample of the air mode, is more than offset by the difference in the Q values. For the DH cavity modes, the difference in the performance for the dielectric and air mode is smaller because the air-mode has a comparatively large Q. Nevertheless, the dielectric mode has the larger M again due to the larger Q, despite the fact that the field and the sample have a very small overlap, four times smaller than for the air mode.

Table 1. The total quality factor, overlap of the field and the sample, figure of merit and modal volume.

Cavity	mode	Q ($\times 10^6$)	f (%)	M ($\times 10^5$)	$V(\lambda/n)^3$
Band edge	air	0.09	44	0.39	2.8
	dielectric	1.3	14	1.8	1.7
Double-heterostructure	air	0.15	16	0.24	2.0
	dielectric	1.2	4	0.48	1.5

We also compare the modal volumes for both modes. The results, obtained using (3), are listed in Table 1. As expected the modal volumes for the dielectric modes are smaller than the volumes for the air modes. However, this difference is not substantial for either of the cavities. Hence PCS cavities are indeed compact sensors, independent of the type of the mode used.

Even though both cavities are designed as a high-Q cavities the results presented here are not exhaustively optimized. It would be possible to increase both the Q and f further, for example by narrowing the waveguide width in the DH type cavity [20]. The overlap of the field and the sample increases monotonically as the waveguide becomes narrower. This is expected as the field, previously mainly concentrated in the waveguide region, penetrates more into holes as the waveguide width is reduced. In this way the fraction of the field in the holes can be significantly increased from 4% for the W1 waveguide to 16% for the $w = 0.70w_{W1}$ waveguide.

4. Optical losses

In reality, both an sample and liquid can induce absorption. This may significantly affect a high-Q cavity performance [16,22]. To quantify this effect we include an imaginary part n_i to the fluid refractive index. In Fig. 3 we plot the resulting figure of merit M as a function of n_i for the two cavities. As the absorption may also be treated perturbatively, the results follow the relation discussed in Ref [23]:

$$\frac{1}{Q_{tot}} = \frac{1}{Q} + \frac{2fn_i}{n_f}, \tag{4}$$

and Q_{tot} falls rapidly once $1/fn_i$ is comparable to the lossless Q.
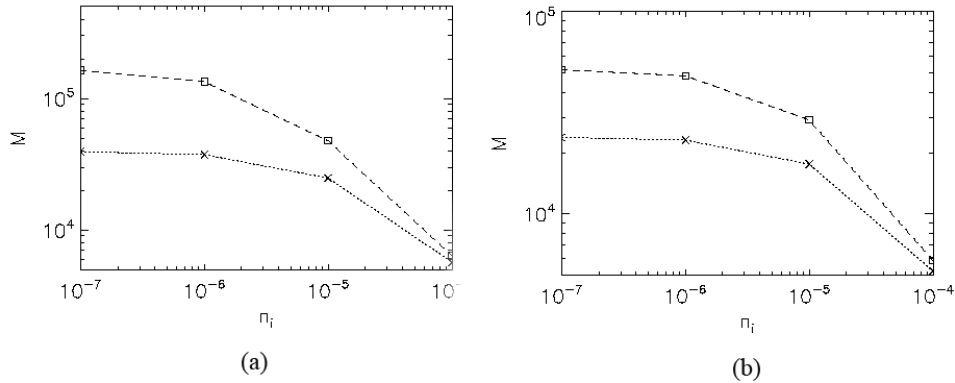

Fig. 3. M as a function of the imaginary part of the refractive index for (a) the band edge cavity and (b) DH cavity for dielectric (squares) and air mode (crosses).

Even though the ratio between the Q of the dielectric and air modes decreases, the figure of merit, M, for the dielectric mode is still larger than M for the air mode in all range considered here. At $n_i = 10^{-4}$ the figure of merit for both modes becomes comparable. In general, one would of course choose to work in a regime with the loss as low as possible, for example at wavelengths below 1μm for aqueous solutions. However, other constraints may force us to tolerate a significant loss, such as fabrication limitations or strong absorption in the PCS material, as is the case for silicon. Therefore one should choose the material composition of the photonic crystal and the fluid hosting the sample according to the wavelength of operation. Dividing Eq. (4) through by f, it is apparent that the merit factor M depends directly on n_i. In other words, the cavity design that has the highest M when the loss is small, continues to have the highest M when losses are present. It is thus reasonable to base design decisions solely on the low loss regime.

5. Conclusions

We have compared the dielectric and air-mode sensitivity for two different types of the PCS cavities. Whilst, the sensitivity of a PC cavity relies on *both* the overlap between the field and the region containing the samples and the quality factor, a good overlap between the field and the fluid has been considered imperative. Our results show that it is not the most crucial factor. This is because the quality factor of the dielectric mode is much larger than that of the air-mode. The larger overlap with the sample of the air mode, is more than offset by the ratio of the Q's. We note that, in general, it is feasible to achieve very high-Q cavities using quite robust designs, while f is highly restricted: typically $f > 0.2$ and it cannot exceed unity. Almost invariably, then, we can expect that optimizing Q at the expense of f is likely to be beneficial, and dielectric bands are thus preferred. Additionally, high-Q PCS cavities are easier to design with dielectric modes than with air modes, and because there already exists a wealth of experience in the fabrication of PC cavities supporting dielectric modes for active devices, our study suggests that dielectric modes, not air modes, are the best suited platform to design PCS sensors. We expect this to hold true for a wide range of cavities beyond the two we have studied here.